Outlook on Marine Propeller Noise and Cavitation Modelling

Artur K. Lidtke[1*], Stephen R. Turnock[1], Victor F. Humphrey[2]

[1]*Fluid Structure Interactions Research Group, University of Southampton, Southampton, SO17 2BJ, UK*

[2]*Institute of Sound and Vibration Research, University of Southampton, Southampton, SO17 2BJ, UK*

Abstract: Two computational studies are presented in this paper. First, the Potsdam Propeller Test Case which is used to demonstrate the capabilities of mass transfer cavitation models, more precisely the model by Sauer and Schnerr, in tackling the problem of marine propeller cavitation. It is shown that the extents of the predicted cavitation regions agree well with the experiment but suffer from the fact that the tip vortices and the associated low pressure regions are under-resolved when URANS is utilised. Next, preliminary results from the study of cavitation noise modelling attempt are presented for a NACA 0009 section, used as a simplified representation of a propeller blade. Large Eddy Simulation and Ffowcs Williams-Hawkings porous acoustic analogy are used in order to estimate the cavitation-induced noise. Results indicate that the discussed approach provides the means for identifying low-frequency noise generation mechanisms in the flow, yielding sound pressure levels of the order of 40 dB re 20 mPa, but does not allow for fine-scale bubble dynamics to be resolved. One may conclude that the discussed approach is a viable option to predict large parts of marine propeller noise spectra but further work is needed in order to account for the high frequency components.

Keywords: Cavitation, noise, large eddy simulation, propeller, acoustic analogy.

1 INTRODUCTION

Concerns about limiting the input of noise into the Oceans have been increasingly more pronounced in recent years. One may associate the anthropogenic noise with multiple mechanisms, shipping being one of the larger contributors (Hildebrand 2009) (Urick 1984). The significance of this is even greater given that a large part of the energy of the ship-related noise falls within the 10-1000 Hz regime and thus has a high potential to affect marine wildlife (Lloyd 2013). Hence, several initiatives have been established in order to investigate how to mitigate the impact of shipping on the marine environment (Van der Graaf et al. 2012) (Tasker et al. 2010).

Apart from the noise due to turbulence, associated, for instance, with local changes of the angle of attack of a propeller blade or shedding of vortices, the noise signature of a marine propeller is significantly affected by cavitation. There are several sources of noise typically induced by this phenomenon. The oscillations of the cavity volume, which may also be seen as an effective change of the blade thickness, typically generate monopole-like. The second major source of cavitation noise may be associated with the collapse and oscillation of individual bubbles (Kirsteins et al. 2011) (Park et al. 2009) (Seol et al. 2005) (Salvatore & Ianniello 2002). The last prominent noise source is the impinging of large scale cavity interfaces upon each other or against solid surfaces (Bensow, R. E., & Bark, G. 2010) Turbulence itself will also contribute to the noise signature of a propeller blade and will interfere with the remaining noise mechanisms (Kirsteins et al. 2011).

It becomes apparent that unsteadiness of the flow will play a crucial role in determining the noise signature of a hydrofoil. Thus, while useful insights may be gained into the cavitation phenomena using approaches such as unsteady RANS or boundary element methods, one should consider using Large Eddy Simulation (LES) to develop a deeper understanding of the underlying flow.

This of particular importance to the project discussed herein, whose main aim is to enable the assessment of the environmental impact of a ship on marine ecosystems by supplying the information about the propeller-induced noise levels. Therefore, the current focus is put on assessing the potential benefits and disadvantages of turbulence and cavitation modelling techniques from the numerical propeller noise modelling perspective.

In order to allow more detailed analysis to be undertaken a basic understanding of the limitations of the modelling methods constituting the current state of the art must be developed. This is done on the example of the Potsdam Propeller Test Case (PPTC). This has seen a significant amount of both experimental and theoretical attention (Abdel-Maksoud 2011), thus becoming one of the more established validation problems. The presented results were obtained using the Schnerr-Sauer mass transfer cavitation model for the flow being solved using unsteady RANS with the $k-\omega$ turbulence model.

The flow over a propeller may be regarded as complex and is thus not very well suitable for preliminary simulations aimed at assessing the cavitation noise. Hence, a simpler test case of a NACA 0009 hydrofoil is also considered, where LES is used instead of RANS to solve the equations of motion of the flow. The far-field sound pressure level is computed using porous Ffowcs-Williams Hawking acoustic analogy implemented in

* *Corresponding author e-mail: akl1g09@soton.ac.uk*

OpenFOAM. The presented analysis focuses on correlating the relationships between the predicted flow features and the corresponding noise signals, allowing for preliminary conclusions to be drawn with respect to the aptness of the presented approach to the modelling of noise of a complete propeller.

2 NUMERICAL MODELLING

2.1 Cavitation Modelling

Cavitation may be described as the transition of liquid into vapour in regions of low pressure. This is caused by the presence of small gas nuclei in the liquid (Plesset & Prosperetti 1977). When subject to tensile stress, these nuclei expand and lead to different types of cavitation, such as sheet or bubble cavitation, depending on the flow conditions (Vallier 2013).

It is possible to simulate the behaviour of individual cavitation bubbles, as described, for instance, by Jamaluddin et al. (2011) and Hsiao & Chahine (2004). However, because of the small size of the cavitation nuclei, ranging between 2 and 50 μm for standard sea water (Woo Shin 2010), it would not be feasible to compute the behavior of every individual bubble in full detail for a flow over a full-scale propeller or a hydrofoil.

For this reason a range of modelling approaches has been introduced in the where one avoids resolving the physics of the bubbles and instead considers the large-scale cavities. One of the alternatives is to model the cavities in the form of a vapour fraction with both the liquid and vapour phases occupying the same physical space and being governed by the same set of equations.

Schnerr-Sauer cavitation model has been used here in order to account for the pressure-induced phase change of liquid into vapour and *vice versa* (Sauer & Schnerr 2001). This is done based on solving the transport equation for a volume fraction, α, with an additional source term introduced on the right-hand side to account for the evaporation and condensation:

$$\frac{\partial \alpha}{\partial t} + \nabla \cdot (\alpha \boldsymbol{U}) = -\frac{\dot{m}}{\rho}. \tag{1}$$

In Equation (1) $\dot{m}$ denotes the rate of change of mass of the liquid-vapour mixture, ρ is the density of the mixture and $\boldsymbol{U}$ is the fluid velocity. The presence of the additional source term also modifies the continuity equation which now becomes

$$\nabla \cdot \bar{\boldsymbol{U}} = \left(\frac{1}{\rho_v} - \frac{1}{\rho_l}\right)\dot{m}, \tag{2}$$

where subscripts v and l refer to vapour and liquid phases, respectively. One may also define the density and viscosity of the liquid-vapour mixture as

$$\begin{aligned} \rho &= \alpha\rho_v + (1-\alpha)\rho_l, \\ \mu &= \alpha\mu_v + (1-\alpha)\mu_l, \end{aligned} \tag{3}$$

respectively.

In order to close the system of equations, an expression for the rate of mass transfer between the liquid and the vapour has to be introduced. In the approach proposed by Sauer and Schnerr this is done by considering the equation of motion of a single bubble of radius R and rearranging it to the following form:

$$\dot{m} = \frac{\rho_l \rho_v}{\rho}(1-\alpha)\frac{3}{R}\sqrt{\frac{2}{3}\frac{(p-p_v)}{\rho_l}}. \tag{4}$$

2.2 Large Eddy Simulation

In the discussed hydrofoil study Large Eddy Simulation (LES) was used in order to model the fluid flow. This approach is based on resolving the most prominent turbulent structures and modelling the remainder of the turbulent kinetic energy spectrum. This is achieved by filtering the momentum equation yielding

$$\frac{\partial \bar{\boldsymbol{U}}}{\partial t} + \nabla \cdot (\bar{\boldsymbol{U}} \otimes \bar{\boldsymbol{U}}) = -\frac{1}{\rho}\nabla \bar{p} + \nu \nabla^2 \bar{\boldsymbol{U}} - \nabla \cdot \boldsymbol{\tau}, \tag{5}$$

were the overbar notation denotes the filtering operation, p is the fluid pressure, and ν is the kinematic viscosity. Similarly, the continuity equation becomes

$$\nabla \cdot \bar{\mathbf{U}} = 0. \tag{6}$$

The non-linear subgrid stress tensor, τ, used to describe the effect of the filtered eddies on the flow in Equation (6), may be expressed as

$$\boldsymbol{\tau} = \overline{\boldsymbol{U} \otimes \boldsymbol{U}} - \bar{\boldsymbol{U}} \otimes \bar{\boldsymbol{U}}. \tag{7}$$

In order to model this quantity one may consider the Boussinesq hypothesis, whereby the stress tensor is assumed proportional to the fluid strain-rate and an assumed subgrid viscosity, ν_{SGS}, yielding

$$\boldsymbol{\tau} - \frac{1}{3}\boldsymbol{\tau} \cdot \boldsymbol{I} = 2\nu_{SGS}\boldsymbol{S}. \tag{8}$$

In the above $\boldsymbol{I}$ is the identity matrix, and the strain rate may be computed as

$$\boldsymbol{S} = \frac{1}{2}(\nabla \bar{\boldsymbol{U}} + \nabla \bar{\boldsymbol{U}}^T). \tag{9}$$

An expression provided by the Smagorinsky model assumes the subgrid scale viscosity to be dependent on a constant coefficient, C_S, and the filter width, Δ, dictated by the mesh density. These yield and expression:

$$\nu_{SGS} = (C_S \bar{\Delta})^2 |\boldsymbol{S}|. \tag{10}$$

2.2 Ffowcs Williams-Hawkings Acoustic Analogy

Ffowcs-Williams Hawkings (FWH) acoustic analogy uses the extended Lighthills equation to predict noise originating from the presence of a turbulent flow (Ffowcs Williams & Hawkings 1969). Based on rearranging the mass and momentum conservation equations of the fluids the acoustic analogy introduces a solution to the inhomogeneous wave equation of the form

$$p'(\boldsymbol{x}, t) = p'_T(\boldsymbol{x}, t) + p'_L(\boldsymbol{x}, t) + p'_Q(\boldsymbol{x}, t), \tag{11}$$

where $\boldsymbol{x}$ and t are the receiver position and time, respectively, p' is the acoustic pressure disturbance, and subscripts T, L and Q refer to the thickness (monopole), loading (dipole) and quadrupole (non-linear) contributions (Lyrintzis 2002) (Ianniello et al. 2012). Each of the terms on the right-hand-side of Equation (11) is computed by evaluating a surface integral of quantities

dependent on the state of the flow. Note that the when a porous formulation is used, as is the case in the presented work, the non-linear term for sources located within the control surface are accounted for via the thickness and loading contributions. This also implies that for such a formulation the monopole and dipole contributions lose their physical meaning (Ianniello et al. 2012).

FWH analogy makes use of two intermediate variables, U_i and L_i . For incompressible flow one may, by definition, neglect the density disturbance. Moreover, when the control surface is stationary the expressions for the acoustic variables may be simplified even further, yielding

$$\begin{aligned} U_i &= u_i, \\ L_i &= (p - p_0)\hat{n}_j + \rho_0 u_i (u_i \cdot \hat{n}_i). \end{aligned} \tag{12}$$

In Equations (12) u_i is the fluid velocity at a point, $\hat{n}$ is a unit vector normal to the control surface, p is the local fluid pressure, p_0 is the reference pressure level, and ρ_0 is the reference fluid density.

For a low Mach number, as is typically the case for a marine propeller blade, the FWH Formulation 2 thickness and loading terms may be computed for a control surface S as

$$4\pi p_T'(\boldsymbol{x}, t) = \int_S \left[\frac{\rho_0 \dot{U}_n}{r}\right]_\tau dS \tag{13}$$

and

$$4\pi p_L'(\boldsymbol{x}, t) = \frac{1}{c_0}\int_S \left[\frac{\dot{L}_r}{r}\right]_\tau dS + \int_S \left[\frac{L_r}{r^2}\right]_\tau dS. \tag{14}$$

Here c_0 denotes the speed of sound in the medium, r is the radiation direction, dot defines a source time derivative, and subscripts r and n refer to the dot product of the quantity in question with a unit vector in either radiation or normal directions, respectively.

In order to account for the fact that the sound contribution of an infinitesimal control surface element will take a finite amount of time to travel between the source and the receiver all of the quantities in Equations (13) and (14) must be evaluated at an appropriate emission time, τ, given by

$$t = \tau + \frac{\boldsymbol{x} - \boldsymbol{y}}{c_0}, \tag{15}$$

where $\boldsymbol{y}$ is the location of the source (integration surface element). In the current implementation of the FWH, developed for the purpose of the discussed project, the control surface is defined by a set cell faces. This provides less control over the density and shape of the control surface than if the flow field was interpolated onto an independent discreet surface. On the other hand, the used approach introduces no additional errors and avoids local pressure and velocity perturbations from being lost.

3 POTSDAM PROPELLER TEST CASE

3.1 Simulation Setup

The discussed controllable pitch propeller has parameters as described in Table 1. The presented work focuses on replicating the conditions from the experimental test case 2.3.1, where cavitation measurements were made for the propeller at the advance coefficient of 1.019, rps-based cavitation number of 2.024 and operating at 24.987 revolutions per second.

The propeller and shaft were treated as no-slip walls with wall-functions applied, velocity inlet and pressure outlet boundary conditions were used to impose the axial flow, with the outer extends of the domain assumed to be slip walls. To match the experimental conditions the water and vapour were taken to have densities of 997.44 and 0.023 kg m^{-3}, respectively, and kinematic viscosities of $9.337 \cdot 10^{-7}$ and $4.273 \cdot 10^{-6}$ kg m^{-2}, respectively. The saturation pressure was taken to be 2818 Pa.

Table 1 Parameters of the Potsdam Propeller.

Radius [m]	0.125	**Eff. Area ratio**	0.779
P/D	1.567	**c at 70% R [mm]**	106.35
No. blades	5	**m at 70% R [mm]**	3.09

Unstructured hexahedral mesh was created using the OpenFOAM snappyHexMesh utility and consisted of 8.8 million cells. Additional refinement was applied around the propeller tips and roots in order to refine the relevant geometry details. Care was taken to ensure that the y+ falls within the logarithmic boundary layer region in order for the wall function models to be valid. A cylindrical domain was considered as it was deemed that modelling the cavitation tunnel walls as present in the experiment would be too expensive computationally. In order to account for the rotation of the propeller a sliding mesh interface was used. An overview of the mesh and domain arrangement is presented in Figure 1.

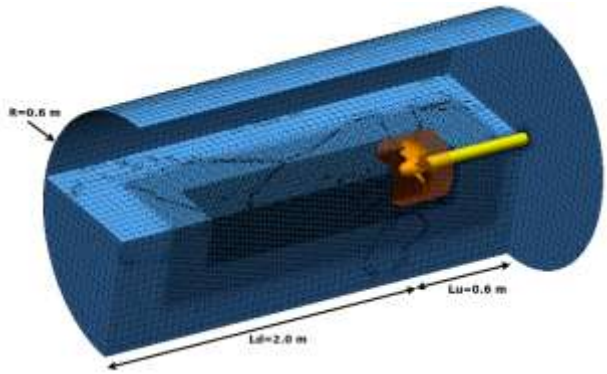

Figure 1 Overview of the domain setup for the PPTC simulation (rotating zone highlighted in orange).

First order time discretisation was used, with the convection term of the RANS equation being resolved using first-second order scheme. First order schemes were used to model the turbulent quantities and van Leer scheme with interface compression was applied to the volume fraction field.

3.2 Results and Discussion

One of the primary considerations for this part of the study was analyzing how well the selected cavitation model predicts the extents of cavitation for a marine propeller operating close to its maximum efficiency point. As shown in Figure 2, a relatively good agreement may be observed between the predicted and measured location of the cavitation regions. One of the immediately apparent drawbacks, however, is the lack of the tip vortex extending downstream of the propeller This is caused by lack of appropriate refinement of the mesh away from the propeller blade and by the fact that RANS methods in general tend to introduce too much dissipation and thus cause the vortices to disappear much sooner than they would in reality.

Despite the mesh being relatively coarse an accurate prediction of the thrust coefficient was achieved in non-cavitating conditions, yielding 0.3740 against the experimental value of 0.3870, i.e. 3.36% relative error. This indicates that the presented method is well suited to provide information useful throughout the propeller design cycle. Unfortunately, unsteady RANS has been recognized as not being able to predict the unsteady behaviour of the cavities particularly well (Bensow, & Liefvendahl2008) (Lidtke et al. 2014), nor is it capable of resolving the tip vortex regions accurately. Both of these phenomena may be expected to play a significant role in the noise generation mechanisms of a marine propeller (Salvatore 2009). It is therefore desirable to use Large Eddy Simulation, or similar high-fidelity turbulence modelling techniques, for the purpose of noise prediction.

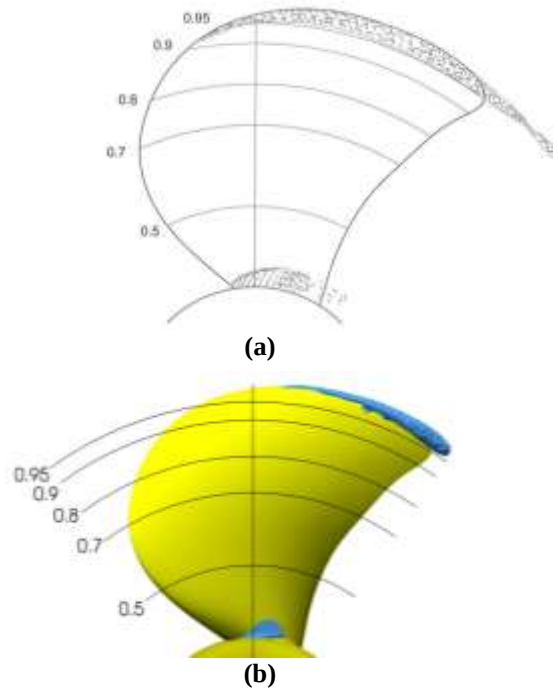

Figure 2 Comparison of the experimental (a) and computed (b) cavitation extents (experimental data from Abdel-Maksoud (2011)).The predicted interface was assumed at volume fraction value of 0.95.

4 NACA 0009 CAVITATION NOISE MODELLING

4.1 Case Setup

Numerical simulations aimed at providing initial noise estimates of a cavitating hydrofoil have been focused on a wing with a NACA 0009 section profile. This was done in order to replicate the conditions used for the Delft Twist 11 foil first presented by Foeth et al. (2006). In said study a wing with a span-wise angle of attack variation symmetric about the mid-span was considered. Here, however, the geometry has been simplified to a fixed span-wise pitch distribution in order to allow a more in-depth study of the sheet cavity behaviour without the added complexity dictated by the complex three-dimensional flow features reported in the original experiments.

The foil with chord of 0.15m, angle of attack of 9^0 and span of 0.05m was placed in the centre of a domain which was to resemble the working section of the cavitation tunnel used by Foeth et al. The domain was chosen to extend 2.5 chord lengths upstream, 4.5c downstream, and was 2.5c wide. The densities of both fluids were taken to be 998 kg m^{-3} and 0.023 kg m^{-3} for water and vapour, respectively, and their corresponding kinematic viscosities were assumed to be 10^{-6} kg m^{-2} and $4.273 \cdot 10^{-6}$ kg m^{-2}. The mean nucleation radius was assumed to be 50 m with the corresponding distribution of 10^8 m^{-3}. Finally, the saturated vapour pressure of the mixture was taken to be 2970 Pa. Speed of sound in water was assumed to be 1500 m s^{-1}.

The control surface used to perform the integration of Equations (14) and (15) has been constructed by expanding the wing section offsets by 0.065m. This distance was chosen so as to avoid any cavities impinging directly onto the surface. Similarly, the downstream extent of the integration surface was chosen to be 0.182m downstream of the trailing edge. The exact placement of the control surface with respect to the wing is depicted in Figure 3.

The inlet was prescribed a fixed velocity of 6.97 m s^{-1} and the simulation was carried out at the cavitation number of 1.07 which was achieved by using a fixed value of pressure at the outlet of 29 kPa (Foeth et al. 2006). Top and bottom of the numerical cavitation tunnel were treated as slip walls and cyclic boundary condition was prescribed to the span-wise boundaries. Convective outlet velocity condition was used in order to limit the amount of reflections being propagated into the domain for the LES simulations. The wing was treated as a no-slip surface and wall functions were used in order to limit the cell count required in the boundary layer region, following the approach outlined by Lu et al. (2010). In order to promote convergence from the early stages of the simulations the runs were initialized from a steady-state, non-cavitating flow solution.

Temporal discretisation has been achieved by the use of a second-order implicit scheme which implied the maximum Courant number limit of 0.5 needed to

maintain stability for LES simulations. The volume fraction was discretised using the van Leer scheme with interface compression and a hybrid convection scheme was adopted in which upwinding is applied when required to maintain stability (Lloyd 2013).

The domain was spatially discretised using a 480x284x40 grid with 5.4 million elements, most of which were concentrated in and near the boundary layer of the foil and between the wing and the FWH integration surface. Special care was taken to ensure that the cavities present would not experience rapid changes in mesh density as they are formed, shed and convected downstream of the foil. Similarly, it was ensured that any flow disturbance moving towards the FWH control surface would not be affected by dissipation errors associated with large changes in mesh topology. The mesh was created using a set of in-house Python libraries combined with the OpenFOAM blockMesh utility. The first wall-normal cell height was ensured to fall within $y+ < 30$, and, to achieve appropriate span- and chord-wise resolution of the flow, the mesh was designed to be characterised by $x+ < 200$ and $z+ < 350$. The grid had been subject to a convergence study whereby the relative change in the predicted steady-state, non-cavitating force coefficients was investigated and found to be less than 2% when compared to a mesh with 9.0 million cells.

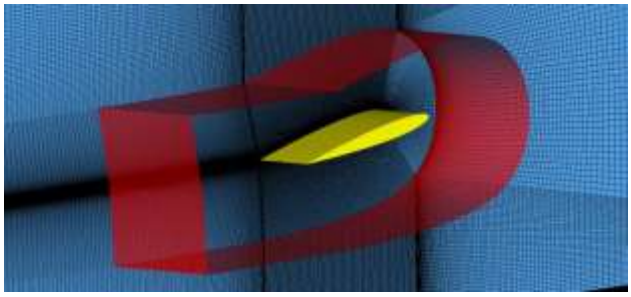

Figure 3 Mesh structure close to the wing (yellow) and the placement of the FWH integration surface (red).

4.2 Results and Discussion

Several receivers were placed around the airfoil in order to record the predicted noise pressure levels. These were located approximately 50 m from the foil and their detailed locations are described in Table 2.

Table 2 Receiver locations

Receiver	x [m]	y [m]	z [m]
0	-c/2	50	s/2
1	0	50	s/2
2	c/2	50	s/2
3	50	0	s/2
4	0	-50	s/2

In order to allow correlation between the recorded noise levels and the predicted flow features the total volume of the cavity was also recorded, together with its extents.

By comparing the chosen parts of the cavity volume and predicted sound pressure levels, Figures 4 and 5, respectively, one may immediately notice that no immediate correlation may be discerned. However, a more in depth analysis of the flow reveals that a new cavity sheet starts to form before a shed cloud becomes disintegrated, as shown in Figure 6. This implies that the maximum volume of the cavity is reached while a cloud is still present in the vicinity of the foil. It thus becomes apparent that, unless the total cavity volume may be broken down into the contribution of the sheet and the clouds, no reliable conclusions may be drawn by comparing the presented data.

It should be mentioned that when compared to a non-cavitating simulation, conducted at cavitation number of 5.0, the presented noise levels are nearly 20 dB re 20 μPa higher. This allows one to deduce that it is the cavitation behaviour and, in particular, that of the cavity sheet that contributes significantly to the noise signature of the presented case. Analysis of the sound pressure levels shown in Figure 5 reveals that there is no significant difference between the sound experienced by receivers spaced radially around the foil. One may thus argue that the noise predicted in this case is of monopole nature, which is expected for a cavity sheet-dominated noise spectrum (Seol et al. 2005).

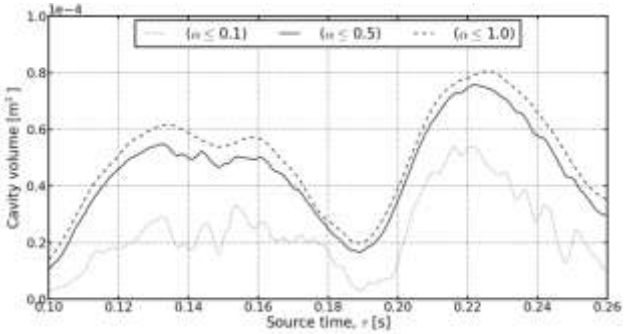

Figure 4 Selected part of the total cavity volume time trace for different volume fraction (α) thresholds.

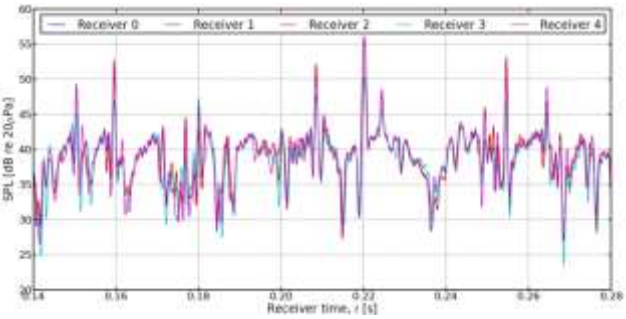

Figure 5 Recorded sound pressure levels for 5 receivers placed in a circumferential manner around the airfoil.

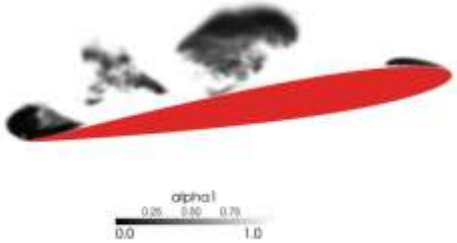

Figure 6 Snapshot of the flow showing formation of a new cavity sheet and the presence of a shed cloud (volume fraction, $\alpha < 1$) downstream of the leading edge.

One may also identify clear peaks in the sound pressure levels in Figure 5. When compared to the state of the flow

at the corresponding emission times, shifted by $\delta t = R_{rec}/c_0 = 0.033\,s$ into the past, these allow several interesting observations to be made. For the peak at $t = 0.16\,s$ a large cloud may be seen to shear off from the downstream edge of the cavity sheet, as shown in Figure 7 (a) and (b). As this takes place the cavity interfaces impact upon each other and generate a localised region of high pressure. As already stated, the presented approached utilises the incompressible flow assumption and, as such, is not well suited to capture this type of flow features but still their impact on the computed sound pressure level may be clearly seen.

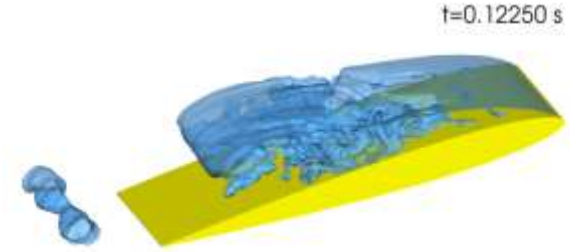

(a)

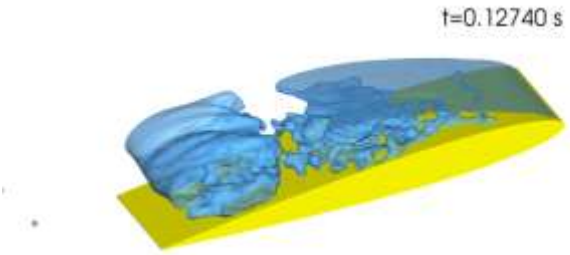

(b)

Figure 7 Shedding of a cavity cloud from the downstream end of the sheet responsible for one of the peaks in the noise signal (receiver time $t = 0.16\,s$).

Next, for receiver time $t = 0.207\,s$ a re-entrant jet may be seen to impact upon the upstream end of the cavity and cause a cloud to be shed, as depicted in Figure 8 (a) and (b). This is a typical mechanism by which sheet cavitation experiences instability and transient behaviour (Lu et al. 2010). One may also see a secondary peak in the noise level just after the primary event, likely associated with the interaction of the turbulence and the shed clouds, causing further interface-interface contact.

(a)

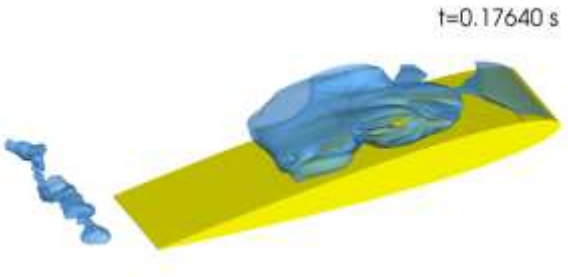

(b)

Figure 8 Necking of the cavity sheet close to the leading edge leading to the shedding of a cloud and the generation of a significant noise peak (receiver time $t = 0.207\,s$).

Finally, for the listener time of $t = 0.22\,s$ one may observe the collapse of a shed cloud following the formation of a re-entrant jet; shown in Figure 9 (a) and (b). While similar to the already discussed behaiviour this event shows a significant amount of three-dimensional nature. It is also interesting to note the visible wake of the jet around the mid-span of the wing and how it causes the cavity to fold over the foil from the sides. The later of the associated snapshots also reveals a complicated cavity structure that this event gives rise to.

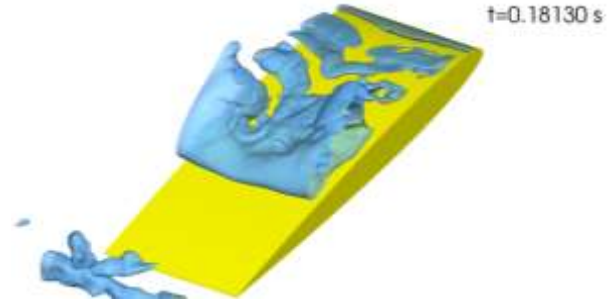

(a)

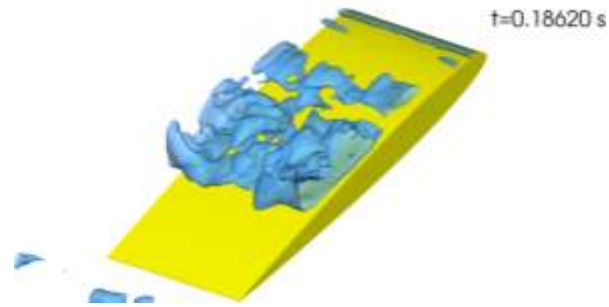

(b)

Figure 9 Complex three-dimensional cavity cloud collapse event following the passing of the re-entrant jet and creating a noticeable noise peak (receiver time $t = 0.22\,s$).

Results presented in Figure 5 also indicate that there is a significant amount of noise present around the foil whose source may not immediately be correlated with particularly obvious significant flow events. One may speculate that this originates from the small-scale oscillations of the cavity interface which induce a local disturbance to the flow. Note should also be taken of the fact that the presence of a cavity sheet effectively modifies the shape of the hydrofoil, leading to highly

turbulent wake, as shown in Figure 10. This is also likely to affect the noise signature.

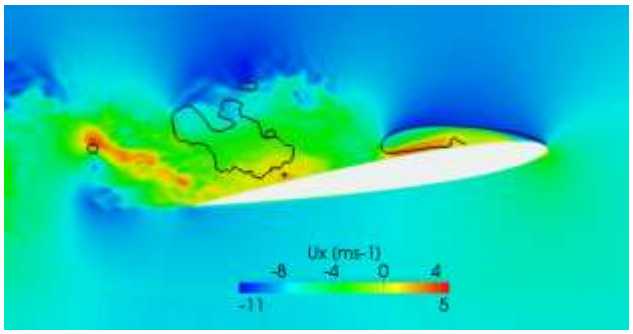

Figure 10 Span-normal cut showing instantaneous axial velocity and volume fraction field iso-contour, $\alpha = 0.9$(black), at $z/s = 0.5$ and simulation time $t = 0.16s$.

5 CONCLUSIONS

It has been shown that appreciably accurate prediction of the cavitation extents may be made for a propeller at a typical loading condition using unsteady RANS combined with a mass transfer cavitation model. This is of particular importance to the designers, who may utilise such cost-effective computational methods in order to support their decision making process. Drawbacks of this method are, however, the inability to resolve the vortical and other turbulent structures accurately. Thus, while it may still be possible to gain substantial insight into the nature of the noise generation mechanisms with said approach, one may be tempted to suffer the increase in computational costs associated with methods such as LES. These offer the potential benefit of substantially increasing the accuracy of the unsteady flow predictions.

The second of the presented studies, focused on the noise analysis of a hydrofoil, has indicated the vast amount of insight that may be gained into the nature of the noise generation mechanisms when high-fidelity turbulence modelling is employed. In particular, the analysis of the presented data has showed that, despite the incompressible treatment of the flow, the noise signature of events such as cloud shedding and re-entrant jet formation may be captured. These have been shown to be the primary noise sources, followed by the noise due to small-scale oscillations of the cavity interface and the noise due to turbulence.

It may thus be concluded that the proposed numerical approach based on a mass transfer cavitation model and acoustic analogy is capable of predicting the low frequency components of the cavitation noise. It suffers, however, from not being able to predict the effect of small bubbles, either shed from the larger cavities or created in the process of bubble cavitation. Moreover, because the fluid is considered to be incompressible, some noise components are expected to be lost from the analysis. In particular, this may be the case for noise associated with formation of shockwaves due to impact of the cavity interfaces against other surfaces.

The above indicatee that the discussed method provides a useful tool allowing greater insight into the nature of cavitation noise but requires further refinement in order to be more reliable.

ACKNOWLEDGMENTS

The authors would like to acknowledge the use of OpenFOAM® libraries and the Iridis 4 supercomputer of the University of Southampton for all of the presented simulations.

REFERENCES

Abdel-Maksoud, M. (ed) (2011), 'Proceedings of the Workshop on Cavitation and Propeller Performance', Second International Symposium on Marine Propulsors - SMP'11, 17 – 18 June, Hamburg, Germany

Bensow, R., & Liefvendahl, M. (2008), 'Implicit and explicit subgrid modeling in les applied to a marine propeller', 38th Fluid Dynamics Conference and Exhibit, pp. 1–12

Bensow, R. E., & Bark, G. (2010). 'Simulating cavitating flows with LES in OpenFOAM', European Conference on Computational Fluid Dynamics, pp. 14–17, Lisbon, Portugal.

Ffowcs Williams, J. & Hawkings, D. L. (1969), 'Sound generation by turbulence and surfaces in arbitrary Motion', Philosophical Transactions of the Royal Society of London Series A, Mathematical and Physical Sciences, vol. 264, no. 1151, pp. 321–342

Foeth, E. J., Doorne, C. W. H., van Terwisga, T., Wieneke, B. (2006), 'Time resolved PIV and flow visualization of 3D sheet cavitation', Experiments in Fluids, vol. 40, pp. 503–513

Hildebrand, J. (2009), 'Anthropogenic and natural sources of ambient noise in the ocean', Marine Ecology Progress Series, vol. 395, pp. 5–20

Hsiao, C.-T., & Chahine, G. (2004), 'Prediction of tip vortex cavitation inception using coupled spherical and nonspherical bubble models and Navier-Stokes computations', Journal of Marine Science and Technology, vol. 8(3), pp. 99–108

Ianniello, S., Muscari, R., and Mascio, A. D. (2012), 'Hydroacoustic characterization of a marine propeller through the acoustic analogy', Sustainable Maritime Transportation and Exploitation of Sea Resources, pp. 991–1000

Jamaluddin, A. R., Ball, G. J., Turangan, C. K., Leighton, T. G. (2011), 'The collapse of single bubbles and approximation of the far-field acoustic emissions for cavitation induced by shock wave lithotripsy', Journal of Fluid Mechanics, vol. 677, pp. 305–341

Kirsteins, I., Clark, P., Atlas, L. (2011), 'Maximum-likelihood estimation of propeller noise modulation

characteristics', Underwater Acoustic Measurements: Technologies and Results

Lidtke, A. K., Turnock, S. R., & Humphrey, V. F. (2014), 'The influence of turbulence modelling techniques on the predicted cavitation behaviour on a NACA0009 foil', Numerical Towing Tank Symposium (NuTTS), Marstrand, Sweden.

Lloyd, T. P. (2013), 'Large eddy simulations of inflow turbulence noise: application to tidal turbines', PhD Thesis, University of Southampton

Lu, N., Bensow, R. E., Bark, G. (2010), 'LES of unsteady cavitation on the delft twisted foil', Journal of Hydrodynamics, Ser. B, vo. 22(5), pp. 784–791

Lyrintzis, A. S. (2002), 'Surface Integral Methods in Computational Aeroacoustics - From the CFD Near-Field to the Acoustic Far-Field', CEAS Workshop "From CFD to CAA", (Athens, Greece), pp. 1–53

Park, C., Seol, H., Kim, K., Seong, W. (2009),'A study on propeller noise source localization in a cavitation tunnel', Ocean Engineering, vol. 36, pp. 754–762

Plesset, M. S. & Prosperetti, A. (1977), 'Bubble dynamics and cavitation', Annual Review of Fluid Mechanics

Salvatore, F. & Ianniello, S. (2002), 'Preliminary results on acoustic modelling of cavitating propellers', IABEM 2002, International Association for Boundary Element Methods, UT Austin, TX, USA

Salvatore, F. (2009), 'Propeller cavitation modelling by CFD-Results from the VIRTUE 2008 Rome workshop',Proc. Of 1st international Symposium on Marine Propulsors, (Trondheim, Norway)

Sauer, J. & Schnerr, G. H. (2001), 'Development of a new cavitation model based on bubble dynamics', Zeitschrift fur Angewandte Mathematik und Mechanik, vol. 81, pp. 561–562

Seol, H., Suh, J.-C., Lee, S. (2005), 'Development of hybrid method for the prediction of underwater propeller noise', Journal of Sound and Vibration, vol. 288, pp. 345–360

Tasker, M. L., Amundin, M. et al. (2010), 'Marine Strategy Framework, Task Group 11 Report: Underwater noise and other forms of energy', European Commission Joint Research Centre, Institute for Environment and Sustainability

Urick, R. J. (1984), 'Ambient Noise in the Sea', Undersea Warfare Technology Office, Naval Sea Systems Command, Dept. of the Navy, Washington D.C.

Vallier, A. (2013), 'Simulations of cavitation-from the large vapour structures to the small bubble dynamics', PhD thesis, Lund University

Van der Graaf, A., Ainslie, M. et al. (2012),'European Marine Strategy Framework Directive: Good Environmental Status (MSFD-GES)', Tech. Rep.

Woo Shin, K. (2010), 'Cavitation simulation on marine propellers', PhD thesis, Technical University of Denmark